Orthopedic Research and Reviews

Dovepress
Taylor & Francis Group

Open Access Full Text Article

ORIGINAL RESEARCH

Identification and Validation of Key Genes Related to Lipophagy in Osteoporosis

Yixin Hu*, Mingliang Zuo*, Yu Wu*, Yu Yang, Xiaobing Shi, Qian Zhang, Ji Wu, Runqi Xie, Yu Bi, Bo Lin, Chou Mo

Department of Orthopedics, The Second People's Hospital of Guiyang, Guiyang, Guizhou, People's Republic of China

*These authors contributed equally to this work

Correspondence: Yu Wu, Department of Orthopedics, The Second People's Hospital of Guiyang, No. 547, Jinyang South Road, Guiyang, Guizhou Province, People's Republic of China, Email 948782069@qq.com

Background: Lipid droplet autophagy (lipophagy) is the breakdown and recycling of lipids within cells via autophagy. Some research suggests that enhancing lipophagy could have potential benefits for bone health. This study aimed to determine the key genes linked to lipophagy in osteoporosis (OP) and provided a reference for the treatment of OP.

Methods: The study analyzed OP-related datasets (GSE56815, GSE62402) and lipophagy-related genes (LRGs). Candidate genes associated with lipophagocytosis were identified through differential expression (DE) analysis and weighted gene co-expression network analysis (WGCNA). The minimum absolute contraction selection operator (LASSO), support vector machine recursive feature elimination (SVM-RFE) and Boruta algorithm are used to identify candidate genes for OP-related feature genes, and the expression of key genes is analyzed. In addition, we constructed a nomogram to predict the incidence of OP patients. Subsequently, multiple bioinformatics tools were used to reveal the associations between key genes and OP. Finally, quantitative real-time polymerase chain reaction (qRT-PCR) was used to detect the expression levels of key genes.

Results: Eight signature genes were identified by machine learning. Only EIF3K and SHMT2 had consistent, significantly different expression trends between OP and control in GSE56815 and GSE62402, being up-regulated in OP. Thus, they were recognized as lipophagy-related key genes. Enrichment analysis showed that EIF3K is related to "Mitochondrial cell assembly", etc., and SHMT2 to "Arf-3 pathway", etc. Both genes negatively linked to activated dendritic cells and mast cells. In regulatory networks, hsa-let-7 family miRNAs were upstream of these genes. Clindamycin and SCHEMBL14520730 targeted them. SHMT2 and EIF3K expression trends matched bioinformatic results.

Conclusion: This study identified lipophagy-related key genes (EI*F*3K and *SHMT2*) in OP, which contributed to the early diagnosis and clinical treatment of OP.

Keywords: lipophagy, osteoporosis, EIF3K, SHMT2, key genes

Introduction

Osteoporosis (OP) is a systemic bone disease caused by a variety of reasons. The main characteristics are decreased bone density and bone quality, damage to bone microstructure, increased bone fragility, and a state prone to fracture. It is a systemic metabolic disorder. In the early stages, some patients may have no obvious symptoms, while others may experience symptoms such as mild pain or decreased activity tolerance.[1] As the disease progresses, especially when a fracture occurs, more obvious symptoms such as pain, reduced height, hunchback, and increased risk of fracture may become apparent.[2] These manifestations can significantly affect the patient's quality of life and mobility. OP is a degenerative disease of the bone that is more common in the elderly and postmenopausal women. With the extension of human life span and the development of an aging society, fractures caused by osteoporosis have greatly increased the disability rate and mortality rate of the elderly and significantly increased the economic burden of social public health.[3] The World Health Organization recommends dual-energy x-ray absorptiometry to measure bone mineral density (BMD)

Received: 17 January 2025
Accepted: 4 June 2025
Published: 22 July 2025

of the spine and proximal femur as a baseline for diagnosing OP and its severity. Due to the insidious onset of OP, patients are often not diagnosed until the first osteoporotic fracture occurs.[4] Therefore, there is an urgent need to find biomarkers that can diagnose OP early, which is essential to initiate treatment before fracture symptoms appear.

Lipophagy is a type of selective autophagy. To prevent excessive accumulation of lipids in cells, cells selectively recognise and degrade cholesterol esters and triglycerides in lipid droplets by activating autophagy- related molecules to produce free cholesterol, fatty acids and glycerol. In this way, it is involved in maintaining intracellular lipid homeostasis and regulating cellular lipid metabolism.[5] Reduced bone strength in postmenopausal osteoporosis patients is usually accompanied by an increase in the amount of adipose tissue in the bone marrow and a decrease in bone mass.[6] In addition, it has been suggested that the presence of fat infiltration in the bone marrow cavity is a result of osteoporosis, especially in menopausal women, and that a possible source of lipid formation in the bone marrow is the disruption of the balance between osteoblasts and fat cell production from bone marrow mesenchymal stem cells, with the latter dominating.[7] Osteoblasts have a phenomenon of lipid droplet accumulation under various pathological and aging conditions, which is further described as an increase in lipid content within the bone cortex, which may lead to the occurrence of age-related OP.[8,9] In particular, recent studies have found that fat autophagy plays an important role in bone metabolism, especially the effect on osteoporosis under high fat conditions.[10] High-fat diet-induced lipid metabolism disorders can alter the bone microenvironment and affect the normal function of bone cells, leading to osteoporosis.[11] Lipoautophagy regulates lipid metabolism and energy balance by degrading intracellular lipid droplets and is essential for maintaining the health of bone cells.[12] Under high lipid conditions, the activation of lipoautophagy can reduce lipid deposition in osteoblasts and alleviate the adverse effects of high lipid environment on osteoblast proliferation and osteogenic differentiation.[13] However, when lipid concentrations are too high, over-activated lipoautophagy inhibits osteoblast proliferation and differentiation, leading to reduced bone formation.[14] In addition, in vivo studies have also shown that activation of lipoautophagy is strongly associated with decreased bone mass in a mouse model of high-fat diet-induced osteoporosis.[15] These results suggest that lipoautophagy plays a complex dual role in bone metabolism, and the maintenance of its balance is of great significance for the prevention of osteoporosis. The above studies indicate that lipophagy is closely related to OP. However, until now, no relevant studies have further explored the specific characteristics and mechanisms of lipid phagocytosis in OP.

To fill this gap, this study employed bioinformatics tools and machine learning algorithms to identify key genes associated with lipoautophagy in osteoporosis. Bioinformatics methods enable comprehensive analysis of large-scale gene expression data to identify potential biomarkers and therapeutic targets. By integrating data from multiple sources, we aim to uncover the underlying molecular mechanisms of lipodroplet autophagy in osteoporosis and provide a theoretical basis for early diagnosis and treatment.

Materials and Methods

Data Source

The OP-related microarray data (GSE56815 and GSE62402) were retrieved from the GEO platform (http://www.ncbi.nlm.nih.gov/geo/), and samples were derived from blood mononuclear cells from subjects who had their BMD measured, with low BMD subjects being considered as OP samples and high BMD subjects being considered as control samples. The GSE56815 dataset (GPL96 platform) included transcriptome data from 40 low BMD and 40 high BMD samples, as well as the GSE62402 dataset (GPL5175 platform) contained transcriptome data from 5 low BMD and 5 high BMD samples. The GSE230665 dataset (GPL10332) contained transcriptome data from 12 low BMD and 3 high BMD samples and was used as a validation set. Additionally, the "REACTOME_LIPOPHAGY" gene set in the Molecular Signatures Database (MSigDB, https://www.gsea-msigdb.org/gsea/msigdb) provided 9 lipophagy-related genes (LRGs), namely PLIN3, PRKAG2, HSPA8, PRKAB1, PRKAG3, PRKAB2, PLIN2, PRKAA2, and PRKAG1.

Weighted Gene Co-Expression Network Analysis (WGCNA)

To identify genes associated with autophagy in lipophagy, WGCNA was performed through WGCNA package (v 1.7.1).[16] Based on all samples of GSE56815 dataset, the single-sample gene set enrichment analysis (ssGSEA) enrichment scores of

the LRGs were computed using "GSVA"-package (v 1.46.0),[17] followed by a violin plot to demonstrate their differences between the OP and control samples. Subsequently, LRG score was utilized as traits to screen for key gene modules by constructing co-expression networks via the "WGCNA"-package (v 1.7.1). Specifically, the samples were analyzed for clustering to examine and remove outliers, with the aim of ensuring the accuracy of subsequent analyses. Next, the soft threshold power (β) from 1 to 20 was set to select the best threshold based on the criterion that the network was close to a scale-free distribution. The clustering tree of the system is derived from the adjacency relationship and similarity between genes, and a co-expression network is constructed according to the criteria of the hybrid dynamic cut tree algorithm. Immediately thereafter, correlation heatmap of trait-module was presented, with particular attention paid to the modules with the highest positive and negative relevance to the trait (LRGs score) and the module genes they contained. Finally, we filtered the above modular genes using gene significance (GS) and module membership (MM), followed by obtaining key module genes with cut-off criteria of |GS|>0.2 and |MM|>0.5.

Differential Expression Analysis and Enrichment Analysis

To identify differentially expressed genes (DEGs) in OP and control samples, differential expression analysis was performed. Specifically, based on the samples in GSE56815 dataset, the identification of DEGs between OP and control samples was implemented using "limma"-package (v 3.54.0),[18] with the cut-off criteria of P.adjust <0.05. The DEGs were demonstrated by generating volcano map and heat map with the "ggplot2"-package (v 3.4.4)[19] and "pheatmap"-package (v 1.0.12),[20] respectively. Subsequently, key module genes were crossed with DEGs to yield DEGs associated with lipophagy, which were recorded as candidate genes.

To elucidate the biological mechanisms of candidate genes, Gene Ontology (GO) annotation and Kyoto Encyclopedia of Genes and Genomes (KEGG) pathway enrichment analyses were implemented via "clusterProfiler"-package (v 4.7.1.003).[21] The threshold was set to P.adjust<0.05.

Machine Learning Algorithms and Expression Level Analysis

For further selection of genes associated with OP, in GSE56815, the candidate genes obtained above were incorporated into machine learning algorithms, including least absolute shrinkage and selection operator (LASSO), support vector machine recursive feature elimination (SVM-RFE), and Boruta, in order to further screen signature genes associated with OP. LASSO analysis was carried out with via the "glmnet"-package (v 4.1–4),[22] where the most important signatures could be efficiently selected by a suitable choice of lambda, sing 10-fold cross-validation to optimize the model performance. Eventually, the LASSO regression selected Lambda.min as the best model. Lambda.min was the Lambda value that minimized the error of the model on the test set during the cross - validation process. The model corresponding to this value performed best in balancing model complexity and prediction accuracy. It could effectively avoid overfitting and ensure that the model had good prediction ability. In addition, in order to further improve the reliability and generalization ability of the model and provide more accurate feature selection results, we applied the Support Vector Machine Recursive Feature Elimination (SVM-RFE) method to the same feature genes and dataset. During the operation, we used the "caret"-package (v 6.0–93) to calculate the weight of each feature. Subsequently, we ranked these features according to their weights.[17] Next, we carried out a 5-fold cross-validation to optimize the model and determine the optimal feature subset. It was used for subsequent analysis and model construction. Boruta algorithm determined the final signature genes by iteratively removing genes of low relevance with the help of the "Boruta"-package (v 8.0.0).[23] The model was iterated 100 times. Each time, a random forest model was used to evaluate the original and shadow features and calculate the scores. Based on these scores, the features were classified into three categories: confirmed, tentative, and rejected. An "importance threshold" was set. When the importance score of an original feature was significantly higher than the 95th percentile of the importance scores of the shadow features, the probability of it being labeled as "confirmed" increased. After 100 iterations, the features that were labeled as "confirmed" multiple times became the important gene set selected by the Boruta algorithm. Immediately thereafter, signature genes from three algorithms were crossed to provide intersecting signature genes.

In addition, the expression levels of these intersecting signature genes between OP and control groups were shown in the GSE56815 and GSE62402 datasets. Importantly, the key genes were selected based on expression stability, so we selected as

key genes those genes that had significant expression differences between the two groups and had consistent expression trends in two datasets. To validate the expression of the key genes, based on the independent dataset GSE230665, we performed a *t*-test using the ggpubr (V 0.4.0) package and plotted a boxplot using ggplot2 to illustrate the gene expression of the samples in the two groups. Finally, Pearson correlation analysis was performed via the "psych"-package (v 2.2.9) (https://www.geeksforgeeks.org/psych-package-in-r/) to reveal relationships between key genes.

Creation of the Nomogram

In order to forecast the incidence of OP patients by integrating key genes, a nomogram was constructed in the GSE56815 dataset via the "rms"-package (v 6.5–0).[22] What's more, calibration curve was created to determine the forecasting ability of nomogram, as well as decision curve analysis (DCA) was employed to assess the utility and validity of nomogram in clinical practice. In addition, ROC curve was generated using the "plotROC"-package (v 2.3.1).[24] Next, based on the GSE230665 dataset, taking whether the samples had the disease as the outcome event, we constructed a nomogram model of the biomarkers using the R package "rms" and generated a ROC curve using the "plotROC" package to evaluate the prediction accuracy of the nomogram.

Gene Set Enrichment Analysis (GSEA)

Enrichment analysis was applied to elucidate the biological pathways in which key genes were involved in OP patients. In this study, based on all samples from the GSE56815 dataset, Spearman-test was accomplished to compute the correlation coefficients between the key genes and the remaining genes, followed by ranking the genes based on the coefficients. Next, the KEGG gene set (c2.cp.v7.2.symbols.gmt) was extracted from the MSigDB as the background gene set, and GSEA was executed via "clusterProfiler"-package (v 4.7.1.003)[21] with the threshold values of |NES|>1, P<0.05, and FDR<0.25.

Immune Infiltration Analysis

To further explore the relationship between OP and immune microenvironment, immune infiltration analysis was performed. Depending on ssGSEA method, our study evaluated the infiltration of immune cells in all samples of GSE56815 dataset via the "GSVA"-package (v 1.46.0),[16] followed by Wilcoxon-test to compare the differential immune cells in OP and control samples. Importantly, we focused more on the relationship between key genes and immune infiltrating cells through completing Spearman-test. Results with |cor|>0.3 and P<0.05 were regarded as remarkably associated.

Construction of Regulatory Networks

To understand the potential regulatory mechanisms of key genes, transcription factors (TFs) regulating key genes were predicted by accessing the ENCODE database based on NetworkAnalyst online platform (https://www.networkanalyst.ca/faces/home.xhtml).[25] In addition, microRNAs (miRNAs) targeting key genes were searched with the help of the TarBase (http://diana.imis.athena-innovation.gr/DianaTools),[26] and subsequently the upstream long non-coding RNAs (lncRNAs) of these miRNAs were yielded by accessing the StarBase (http://starbase.sysu.edu.cn/).[27] Regulatory networks of TF-mRNA and lncRNA-miRNA-mRNA were generated via Cytoscape software (v 3.9.1).[28]

Drug Prediction and Molecular Docking

This study accessed the Drug Signatures database (https://dsigdb.tanlab.org/DSigDBv1.0/) to predict drugs targeting key genes and to analyze their interactions, with the aim of facilitating accurate drug prediction and informing therapeutic interventions. Following this, the top 10 drugs were demonstrated based on the ranking of drug-key gene interaction scores, as well as the binding energy (BE) between these 10 drugs and key genes was calculated with the use of the CB-Dock online molecular docking tool (https://cadd.labshare.cn/cb-dock/php/blinddock.php). It was generally accepted that their interaction was stable when BE < −5 kcal/mol.

What's more, we chose the drugs that acted most stably with the key genes to further explore the docking patterns between them. Specifically, the 3D structure of the drug and the crystal structure of the key gene-encoded protein were downloaded using PubChem website (https://pubchem.ncbi.nlm.nih.gov/) and UniProt website (https://www.uniprot.org/),

respectively. Docking experiment was then performed through the CB-Dock online molecular docking tool, followed by visualization of the docking results using the PyMOL software (v 3.1.1).[29]

Quantitative Real-Time Polymerase Chain Reaction (qRT-PCR)

We collected whole blood samples from 5 OP patients and 5 normal subjects for qRT-PCR to verify the expression levels of key genes. The experiment was approved by the Ethics Committee of The Second People's Hospital of Guiyang (approval number: JYYY-2024-WZ-15).

According to the manufacturer's protocol, total RNA was extracted from blood samples using TRizol reagent (Ambion). The cDNA was subsequently synthesized by reverse transcription of mRNA using the SweScript First Strand cDNA Synthesis Kit (Wuhan Servicebio Technology Co., Ltd). A total of 40 cycles of reaction were carried out with the aid of the CFX96 Real-Time Quantitative PCR System: 95°C for 1 minute, 95°C for 20 seconds, 55°C for 20 seconds, and 72°C for 30 seconds. The primer sequences were listed in Table 1. Relative expression of gene was calculated using the $2^{-\Delta\Delta Ct}$ method with GAPDH as the reference gene. GraphPad Prism 5 was used for graphing and statistical analysis.

Statistical Analyses

R software was used for all statistical analyses. Differential expression analysis was performed using the "limma" package (v3.54.0). Differential expression analysis was performed using the "limma" package (v3.54.0). Weighted Gene Co-expression Network Analysis (WGCNA) was performed using the "WGCNA" software package (v1.7.1). The Minimum Absolute Contraction and Selection Operator (LASSO) is implemented using the "glmnet" package (v4.1–4). Support vector machine recursive feature removal (SVM-RFE) was performed using inserted symbol packs (v6.0–93), and low-correlation genes were iteratively removed using Boruta algorithm (v8.0.0). The analysis of functional enrichment was carried out using the "clusterProfiler" package. Additionally, ROC curves were plotted using the "plotROC" package, and nomograms were constructed using the "rms" package. Genset enrichment analysis (GSEA) was performed using the "clusterProfiler" software package (v4.7.1.003), using the KEGG gene set as the background gene set, and the threshold was set to$|NES| > 1$, $P < 0.05$, $FDR < 0.25$. Immune infiltration analysis was conducted using the "GSVA" package (v1.46.0), and Spearman correlation coefficients were used for correlation analysis.

Results

The flowchart of the data processing steps for the results of this study is shown in Supplementary Figure 1.

The 285 Key Module Genes Were Obtained Through WGCNA

In GSE56815 dataset, the LRGs score between OP and control samples were significantly different, with significantly higher score in OP samples ($P < 0.05$) (Figure 1a). With respect to WGCNA, the results of the cluster analysis indicated that no outlier was found (Figure 1b). When β was equal to 7, the scale-free topological fit index was greater than 0.85 (red line) and the mean connectivity tended to zero (Figure 1c). Based on correlation clustering, nine gene modules were classified and assigned different color labels (excluding grey) (Figure 1d). Among them, the MEgreen had the highest positive relevance to LRGs score (cor=0.46 and P<0.001) and the MEmagenta had the highest negative relevance to LRGs score (cor=−0.33 and P=0.003) (Figure 1e). Eventually, 285 genes included in MEgreen and MEmagenta that met the criteria of |GS|>0.2 and |MM|>0.5 were determined to be key module genes highly correlated with the LRGs score (Figure 1f).

Table 1 RT-qPCR Primer Sequence List

Gene	Forward Primer	Reverse Primer
EIF3K	AGCCTTCTTTCAGACCACGG	AGCTGGCTGTACTTTCGGAC
SHMT2	GCACAGTGGGGAGTCAATGT	GTCAGTGCCAGGTTGAGCTTAT
GAPDH	CGAAGGTGGAGTCAACGGATTT	ATGGGTGGAATCATATTGGAAC

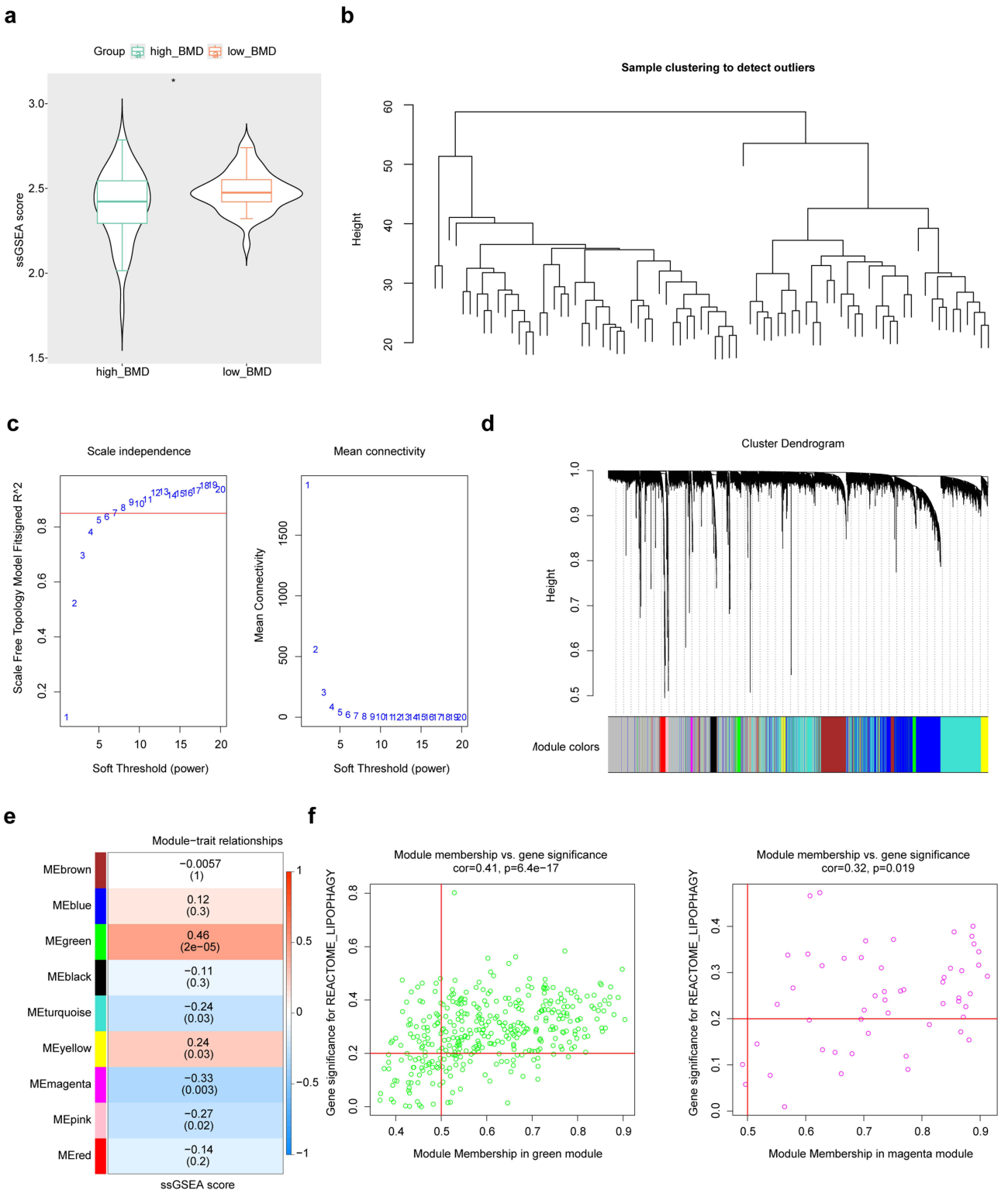

Figure 1 WGCNA screening for key module genes. **(a)** Plotting ssGSEA scores between low BMD and high BMD; * $p < 0.05$. **(b)** Sample level clustering tree to remove outlier samples. **(c)** Screening for soft thresholds. **(d)** Identify co-expression modules. **(e)** Heat map of correlation between co-expression modules and ssGSEA. **(f)** Screening for key modules.

https://doi.org/10.2147/ORR.S518036

Identification of 28 Candidate Genes and Enrichment Analysis

In GSE56815 dataset, there were 2,613 DEGs between the OP and control controls, including 1,766 up-regulated and 847 down-regulated genes in OP samples (Figure 2a and b). Subsequently, the Venn diagram illustrated 28 candidate genes by overlapping 2,613 DEGs and 285 key module genes (Figure 2c).

These 28 candidate genes were enriched and analyzed, yielding 426 GO entries [318 biological processes (BPs), 54 cellular components (CCs), and 54 molecular functions (MFs)] and 10 KEGG signaling pathways (P.adjust < 0.05). With respect to GO, the top 10 entries were mainly related to "box C/D snoRNP assembly", "small nucleolar ribonucleoprotein complex assembly", "RPAP3/R2TP/prefoldin-like complex", "mitochondrial inner membrane", "oxidoreductase activity, acting on the CH-CH group of donors", and so on (Figure 2d). KEGG analysis elucidated that candidate genes were engaged in "Peroxisome", "Phagosome", "Natural killer cell mediated cytotoxicity", etc. (Figure 2e).

EIF3K and SHMT2 Were Determined to Be Key Genes in OP

The LASSO algorithm yielded 14 signature genes associated with OP at optimal lambda = 0.0349289 and when the coefficients of the genes were not penalized to zero, including *RAC1, EIF3K, RUVBL2, PTAFR, SNX1, HLA*-E, *SHMT2, CARKD, COX20, NIT1, VPS72, COQ9, ATRIP*, and *RNH1* (Figure 3a). The SVM-RFE algorithm selected the model with the highest accuracy, containing 24 signature genes (Figure 3b). Furthermore, Boruta analysis selected 12 signature genes based on each signature's importance (Figure 3c). Next, the overlapping analysis of the signature genes obtained by the three algorithms, resulting in eight intersecting signature genes, namely *RAC1, EIF3K, RUVBL2, PTAFR, HLA*-E, *SHMT2, NIT1*, and *RNH1* (Figure 3d).

What's more, the GSE56815 and GSE62402 datasets were utilized to conduct the expression analysis of these genes, which revealed that *EIF3K* and *SHMT2* significantly differed between the OP and control groups (P < 0.05) and were all considerably up-regulated in OP samples (Figure 3e and f). At the same time, we conducted an expression level validation based on the dataset GSE230665. The results showed that both EIF3K and SHMT2 were significantly more highly expressed in the OP group than in the other group among the two groups (p < 0.01), which was consistent with their expression patterns in the training group (Supplementary Figure 2a and b). Therefore, *EIF3K* and *SHMT2* were considered key genes associated with lipophagy in OP. Notably, the expression levels of *EIF3K* and *SHMT2* were remarkably positively correlated (Figure 3g).

Building an Effective Nomogram for Diagnosing OP

We constructed a nomogram model in GSE56815 dataset in order to facilitate the clinical use of selected two key genes to predict the occurrence of OP (Figure 4a). The slope of the calibration curve approached 1 and the AUC value in the ROC curve was greater than 0.7, implying that the accuracy of the nomogram in forecasting OP was favorable (Figure 4b and c). The DCA results showed that the nomogram produced a net benefit (Figure 4d); in other words, the nomogram had a high degree of clinical utility. Meanwhile, based on the independent validation set of GSE230665, a nomogram model was constructed (Supplementary Figure 2c). The AUC value of the ROC curve was 0.972, which indicated that the nomogram had good accuracy in predicting OP (Supplementary Figure 2d).

Multiple Enrichment Pathways for Key Genes Were Explored

To further elucidate the signaling pathways linked to the two key genes, GSEA was performed in GSE56815 dataset. The genes *EIF3K* and *SHMT2* were enriched in 319 and 201 KEGG pathways, respectively. The top 5 pathways were selected for visualization based on enrichment score ranking. The results indicated that *EIF3K* was remarkably linked to "SM pathway", "PECAM-1 interaction", "Electron transport chain in mitochondria", "Mitochondrial cell assembly", and "Oxidative phosphorylation" (P < 0.05) (Figure 5a). *SHMT2* expression was significantly correlated with "Arf-3 pathway", "Mitotic telophase cytokinesis", "Transport of nucleosides, free purines and pyrimidine bases on the plasma membrane", "VLDLR internalization and degradation", and "H19 action Rb-E2F1 signaling and CDK beta-catenin activity" (P < 0.05) (Figure 5b). These analyses indicate that key genes are highly associated with these biological pathways, providing valuable insights into the underlying molecular mechanisms of OP.

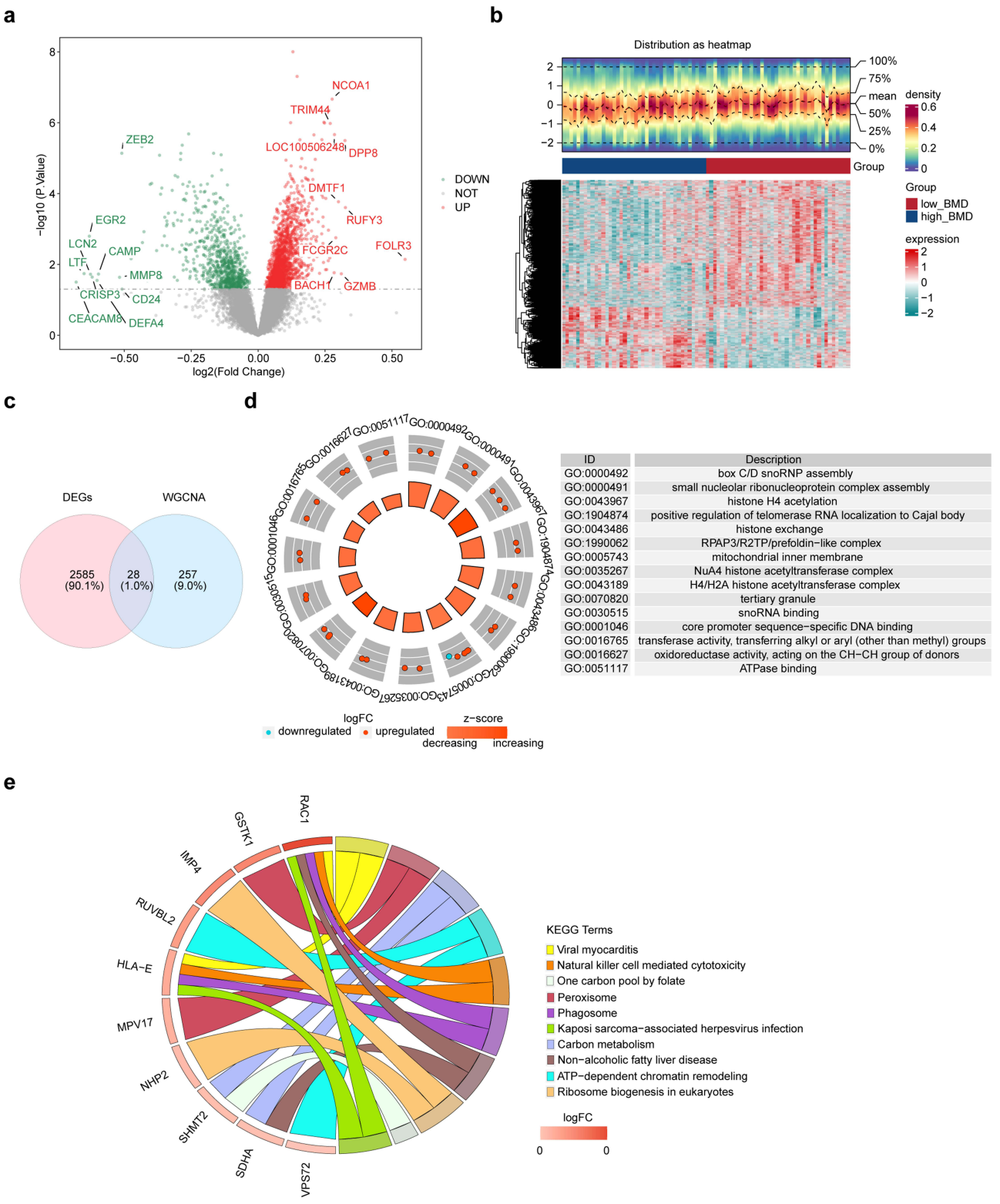

ID	Description
GO:0000492	box C/D snoRNP assembly
GO:0000491	small nucleolar ribonucleoprotein complex assembly
GO:0043967	histone H4 acetylation
GO:1904874	positive regulation of telomerase RNA localization to Cajal body
GO:0043486	histone exchange
GO:1990062	RPAP3/R2TP/prefoldin−like complex
GO:0005743	mitochondrial inner membrane
GO:0035267	NuA4 histone acetyltransferase complex
GO:0043189	H4/H2A histone acetyltransferase complex
GO:0070820	tertiary granule
GO:0030515	snoRNA binding
GO:0001046	core promoter sequence−specific DNA binding
GO:0016765	transferase activity, transferring alkyl or aryl (other than methyl) groups
GO:0016627	oxidoreductase activity, acting on the CH−CH group of donors
GO:0051117	ATPase binding

Figure 2 Identification and enrichment analysis of DE-LRGs. **(a)** Volcano mapping of differentially expressed genes between OP and control samples. Green represents downregulated genes, red represents upregulated genes, and gray represents genes with no significant differential expression. **(b)** Heat map of differentially expressed genes between OP and control samples. **(c)** Venn diagram of DE-LRGs. **(d)** Plot of GO enrichment results of DE-LRGs. **(e)** Plot of KEGG enrichment results of DE-LRGs.

https://doi.org/10.2147/ORR.S518036

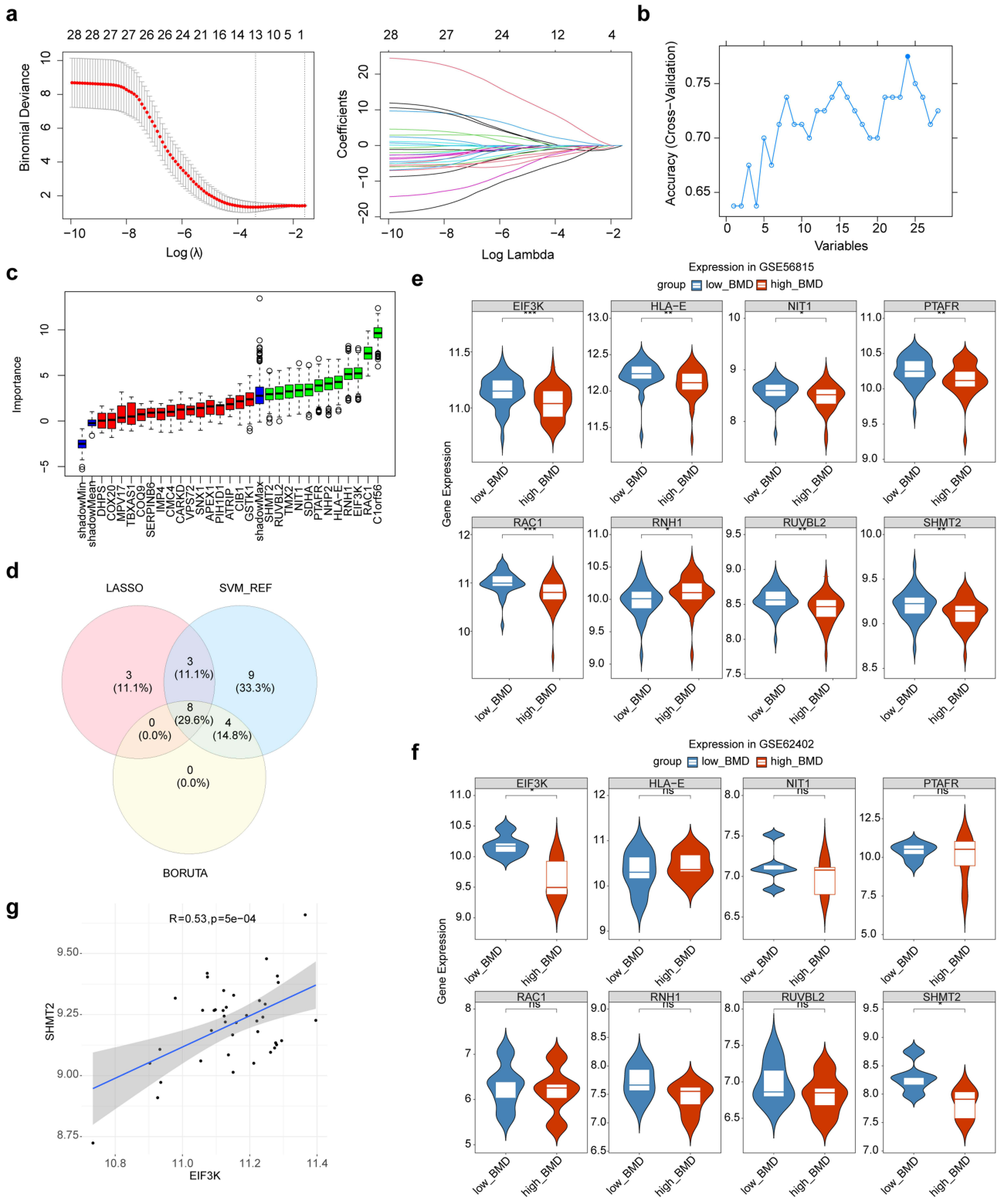

Figure 3 Screening of key genes in OP. **(a)** The LASSO logistic regression coefficient penalty plot. **(b)** Accuracy of the model under different features. **(c)** Boruta algorithm to identify candidate key genes. **(d)** Venn diagram of candidate genes. **(e)** Plotting the expression violin of candidate genes in OP group and control group (training set GSE56815); * $p < 0.05$; ** $p < 0.01$; *** $p < 0.001$.**(f)** Plotting the expression violin of candidate genes in OP group and control group (validation set GSE62402); * $p < 0.05$; ** $p < 0.01$; *** $p < 0.001$. **(g)** Correlation scatter plot of expression levels of key genes. ns, not significant.

https://doi.org/10.2147/ORR.S518036

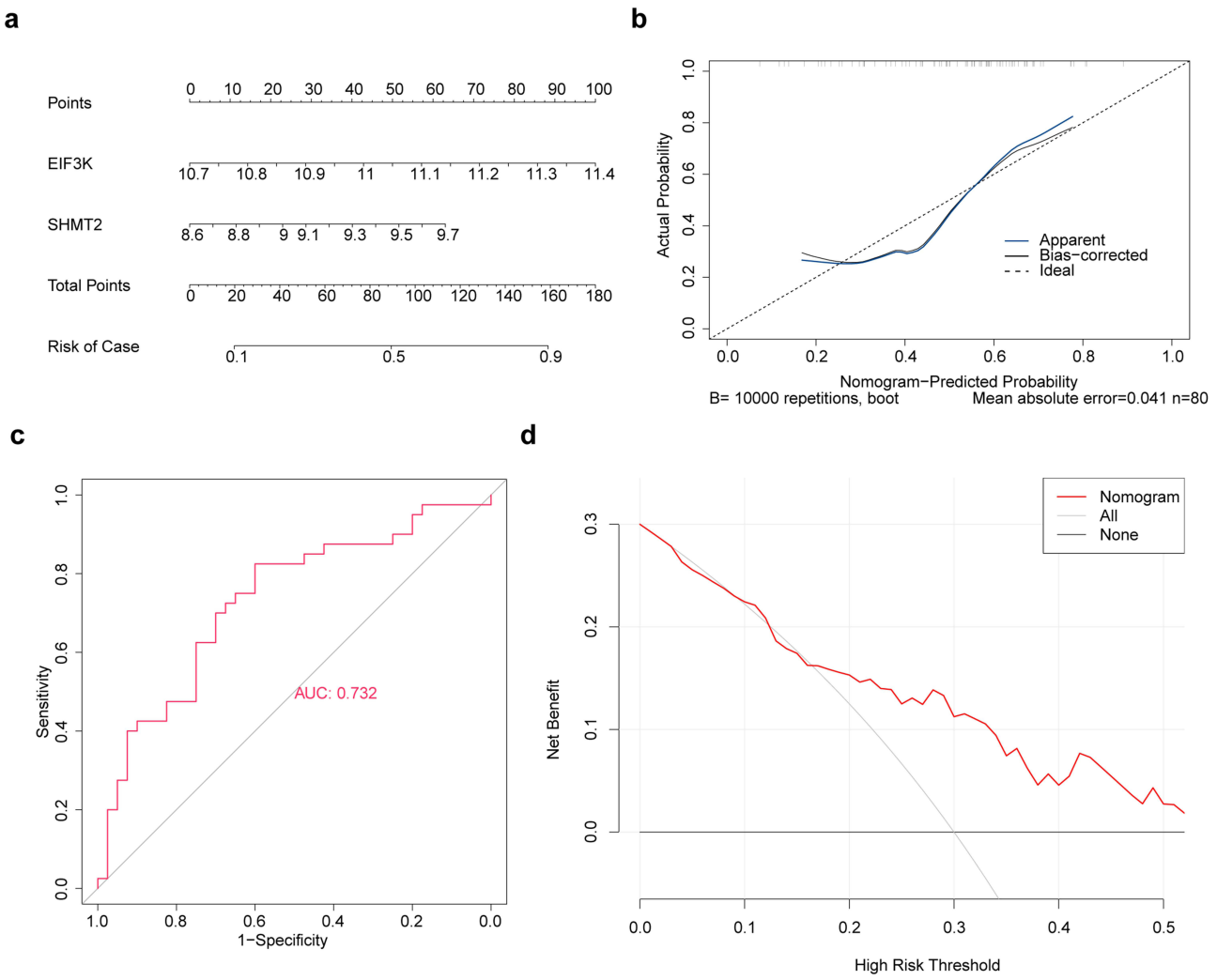

Figure 4 Construction of Nomogram. **(a)** Nomogram modelling of biomarkers. **(b)** Plotting calibration curves to assess the accuracy of Nomogram predictions. **(c)** Plotting ROC curves to assess the accuracy of Nomogram predictions. **(d)** Plotting decision curves to assess the accuracy of Nomogram predictions.

Key Genes Were Linked to Immune Infiltrating Cells in OP

The infiltration abundance of 28 types of immune cells in OP and control groups of the GSE56815 dataset was shown in Figure 6a. Among them, the activated dendritic cells and mast cells were significantly different between the OP and control groups, and both of them were down-regulated in the OP samples ($P < 0.05$) (Figure 6b). Furthermore, Spearman correlation demonstrated that both *EIF3K* and *SHMT2* were significantly positively linked to CD56dim natural killer cells (cor>0.3, P<0.001), while significantly negatively linked to immature B cell (cor<-0.3, P<0.001) (Figure 6c and d). What's more, we could observe that both key genes were negatively correlated with two differential immune cells (activated dendritic cells and mast cells) identified. In summary, these immune cells might have an impact on the development of OP by influencing key genes.

Key Genes Were Regulated by Multiple Molecules

A total of 88 TFs were predicted, including 47 TFs targeting EIF3K and 61 TFs targeting SHMT2, and the network of TF-key genes was displayed in Figure 7a. It could be found that 20 TFs (ZNF324, ZNF76, ZNF71, ZNF2, ZNF143, etc.) could regulate two key genes simultaneously. Furthermore, 77 miRNAs and 24 lncRNAs were predicted based on public databases, of which 59 miRNAs targeting SHMT2 and 28 miRNAs targeting EIF3K. In lncRNAs-miRNAs-mRNAs network, multiple relationship pairs were found (Figure 7b), such as, lncRNA (STAG3L5P-PVRIG2P-PILRB) could regulate EIF3K expression via miRNAs (hsa-miR-16-5p, hsa-miR-15b-5p, and hsa-miR-424-5p), as well as the miRNAs of the hsa-let-7 family (hsa-let

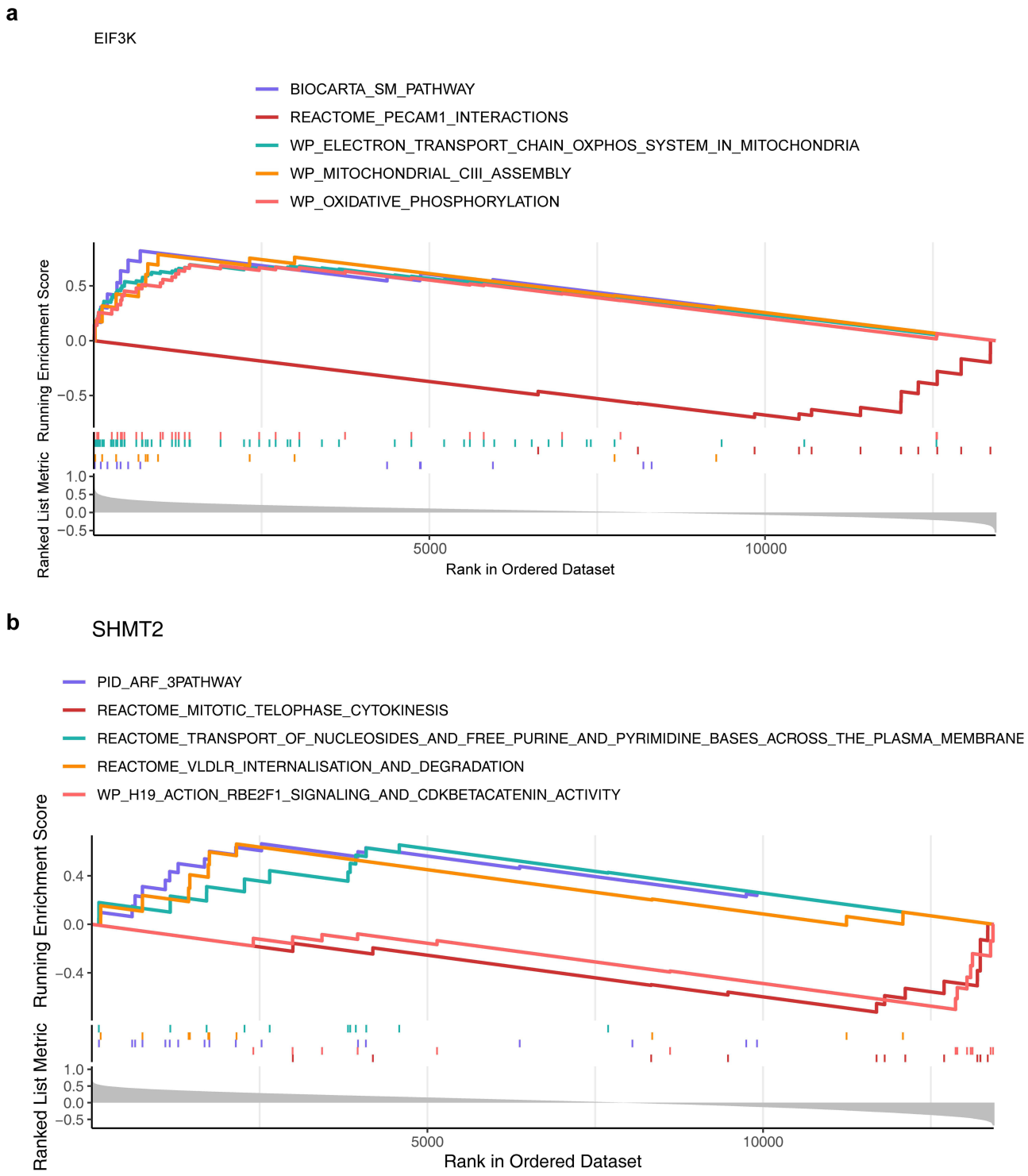

Figure 5 GSEA enrichment analysis of key genes. **(a)** Graphical representation of KEGG enrichment analysis results for *EIF3K*. **(b)** Graphical representation of KEGG enrichment analysis results for *SHMT2*.

-7a-5p, hsa-let-7b-5p, hsa-let-7d-5p, hsa-let-7e-5p, hsa-let-7f-5p, hsa-let-7g-5p, and hsa-let-7i-5p) were important upstream miRNAs for two key genes, implying that these might be important therapeutic targets for OP.

https://doi.org/10.2147/ORR.S518036

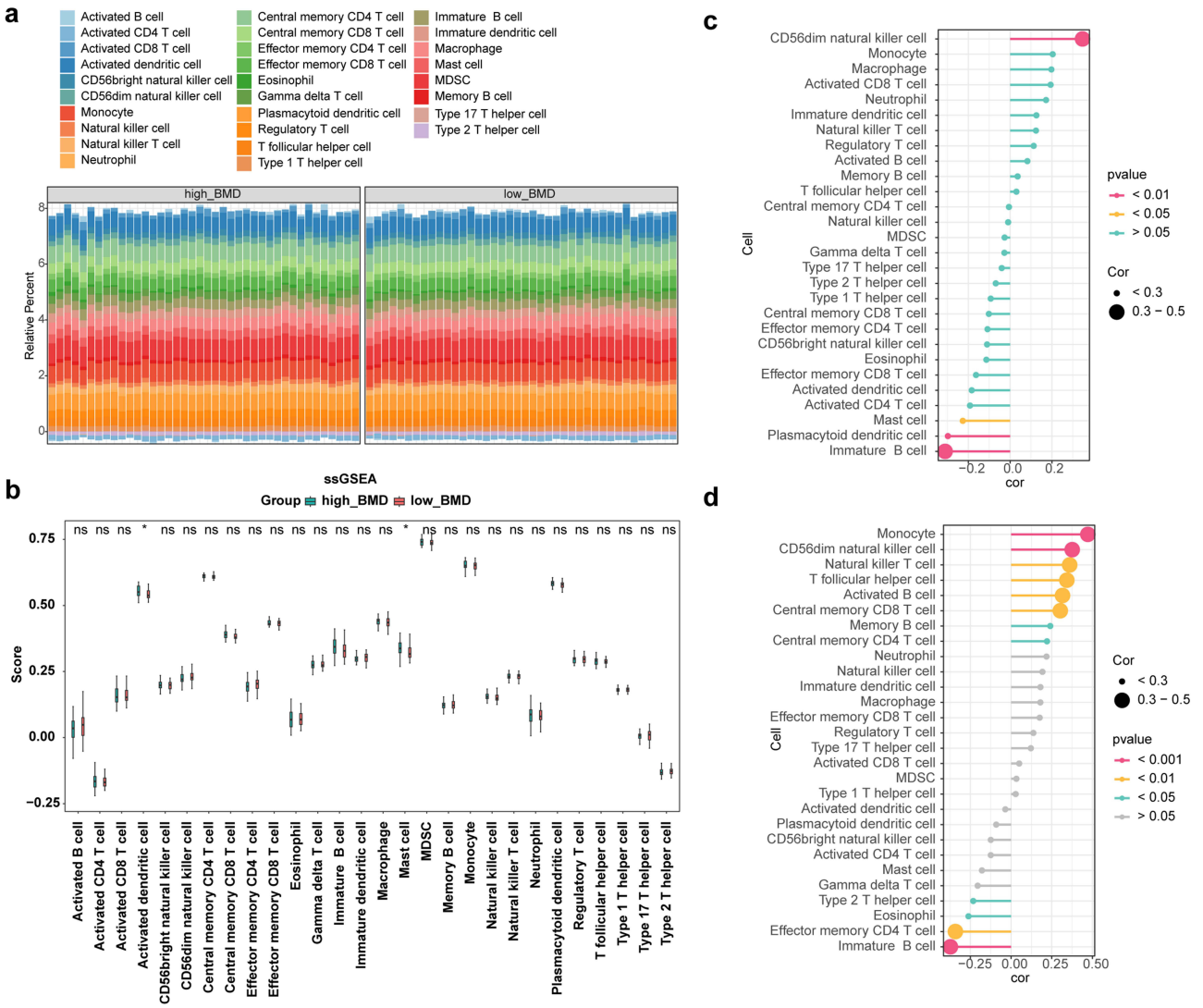

Figure 6 Immune infiltration analysis of key genes. **(a)** Plotting 28 immune infiltrating cells in high BMD and low BMD situation box lines. **(b)** Differences in immune infiltrating cells between high BMD and low BMD. ns, not significant; *, $p < 0.05$. **(c-d)** Correlation analysis of key genes and immune infiltrating cells.

Key Genes Had Good Binding Effects with Predicted Drugs

Through a thorough analysis of the DSigDB database, 29 drugs were retrieved, including four drugs targeting *EIF3K* and 27 drugs targeting *SHMT2* (Figure 8a). Of these, clindamycin and SCHEMBL14520730 were common drugs that targeted two key genes. The top 10 drugs selected on the basis of the drug-key gene interaction score were considered to be potential drugs that could be used to treat OP and for subsequent analyses. These 10 potential drugs included SCHEMBL14520730, clindamycin, uracil, pyridoxal phosphate, methylergometrine, primidone, valinomycin, benserazide, NSC25485, and DL-METHIONINE (Table 2).

In addition, the molecular docking results indicated that the BE values of most of the drugs to the key genes were less than −5 kcal/mol (Table 3), implying that their interactions were stable We were particularly interested in the molecular docking patterns between the most active drugs and the corresponding key genes. However, no interacting hydrogen bonds were found in EIF3K-SCHEMBL14520730, so we visualized the molecular docking patterns of EIF3K-NSC25485 and SHMT2-SCHEMBL14520730 (Figure 8b and c).

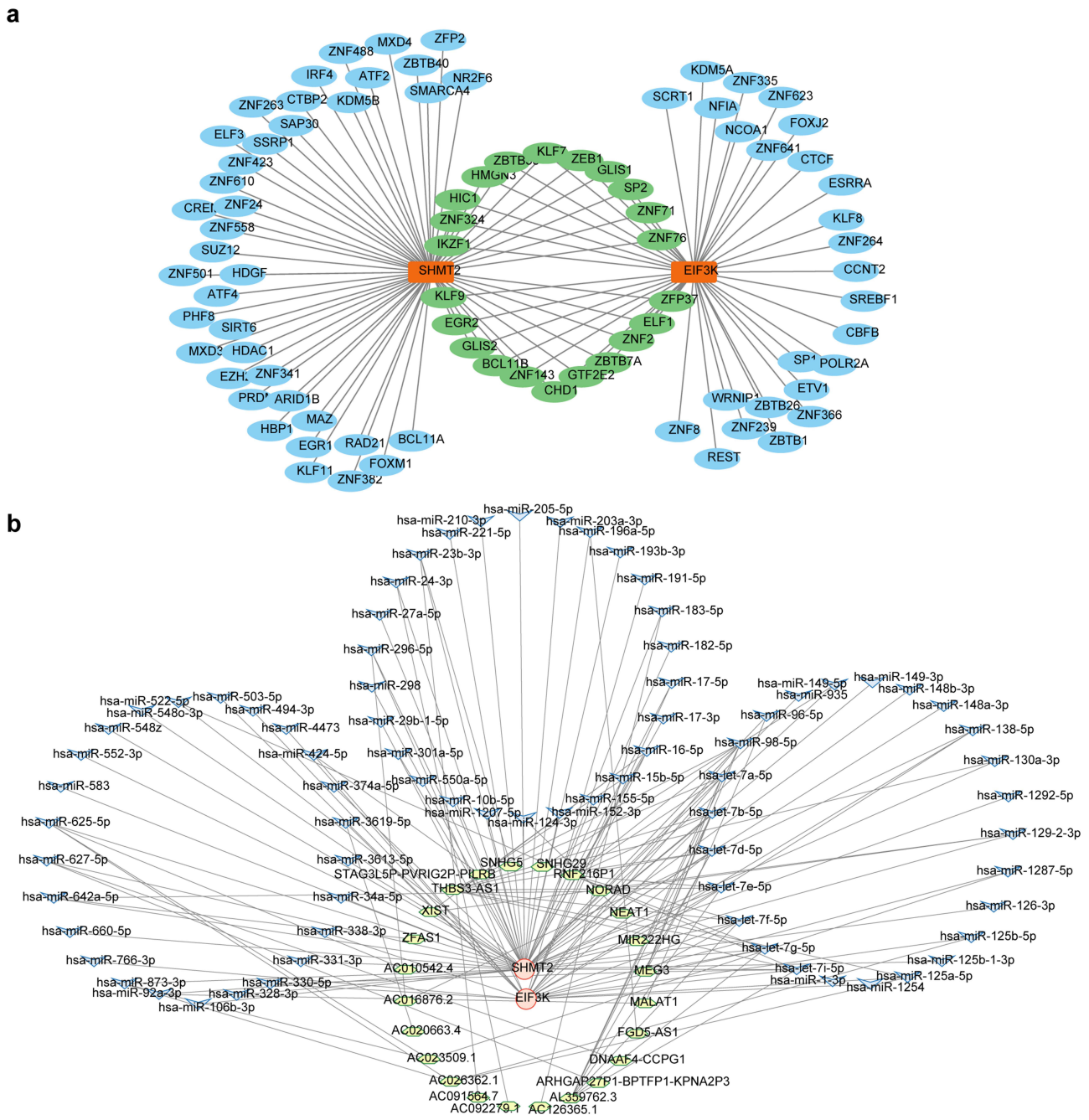

Figure 7 Construction of regulatory network. **(a)** Diagram of the TF regulatory network of key genes. Orange: key genes; green: transcription factor TFs common to key genes; blue: transcription factor TFs of individual key genes. **(b)** Construction of ceRNA network diagram. Orange is mRNA; blue is miRNA; green is lncRNA.

Expression of SHMT2 and EIF3K Was Different in Control and OP Samples

With respect to the qRT-PCR results, the expression of *SHMT2* was found to be significantly different between OP and control samples (P = 0.034) (Figure 9a), with higher expression in OP samples, which was consistent with the bioinformatics results. However, *EIF3K* expression was not significantly different (P > 0.05) between the OP and control groups (Figure 9b), which may be attributable to the small sample size.

https://doi.org/10.2147/ORR.S518036

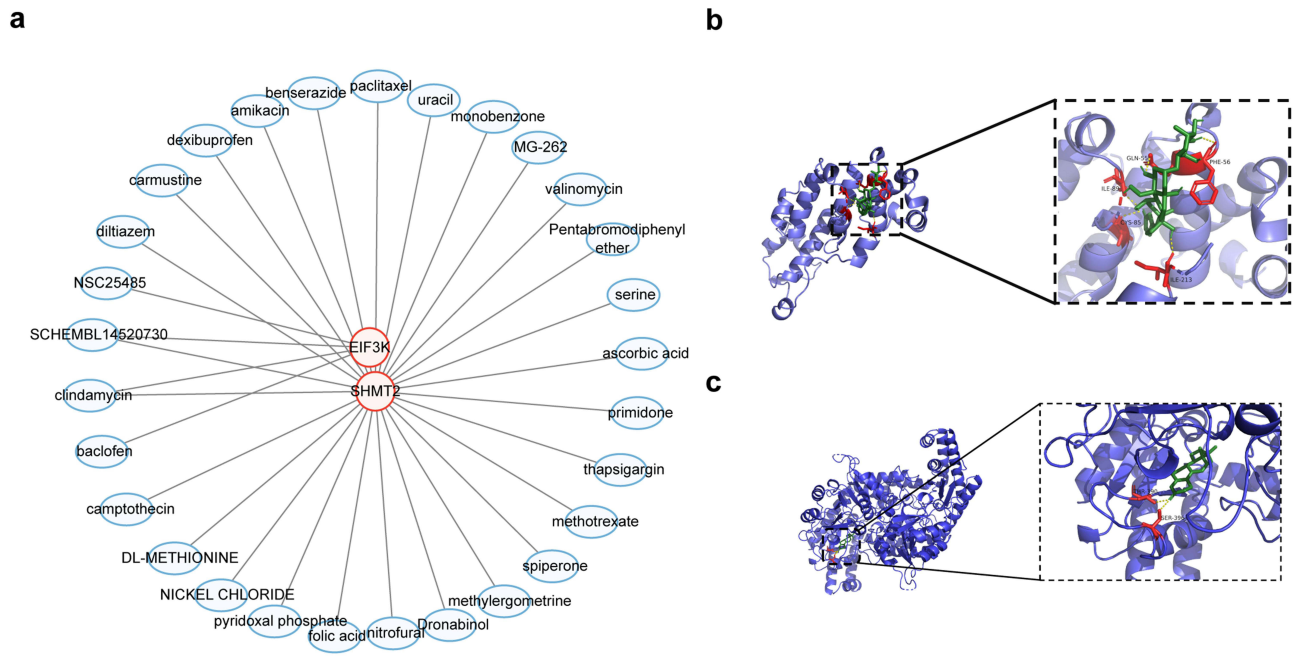

Figure 8 Drug prediction and molecular docking. **(a)** Drug-key gene interaction network. Key genes in Orange; targeted drugs in blue. **(b)** Molecular docking pattern of NSC25485 with the corresponding protein of *EIF3K*. **(c)** Molecular docking pattern of NSC25485 with the corresponding protein of *SHMT2*.

Discussion

OP is a common disease associated with aging. Autophagy plays a crucial role in maintaining bone homeostasis, and the changes in this pathway are related to the occurrence of osteoporosis to a certain extent.[30,31] It has been confirmed that inhibiting autophagy of osteoclasts can inhibit bone mass loss to a certain extent.[32–34] However, the molecular mechanism of lipophagy in OP remains unclear, and reliable biomarkers are lacking in the absence of obvious symptoms in the early stages of OP. Therefore, it is necessary to further explore the molecular mechanisms of lipid phagocytosis in OP. In this study, we identified two key genes, eukaryotic translation initiation factor 3K (EIF3K) and serine hydroxymethyltransferase 2 (SHMT2), through bioinformatic methods. These genes may play an important role in the pathogenesis of OP and provide an important reference for early diagnosis and prevention of OP.

SHMT2 is a mitochondrial enzyme that is essential for mitochondrial function and may influence osteoporosis through its role in mitochondrial homeostasis.[35] The deletion of SHMT2 in human cells or mice can lead to blocked translation of respiratory chain complex proteins in mitochondria, respiratory chain dysfunction, and low oxidative phosphorylation efficiency.[36,37] All these evidences suggest that SHMT2 plays an important role in the maintenance of

Table 2 Potential Drugs for OP

Drug Name	Combined Score	Molecular Formula
SCHEMBL14520730	314,087.1803	C19H24O2
Clindamycin	184467.4536	C18H33ClN2O5S
Uracil	4348.372853	C4H4N2O2
Pyridoxal phosphate	4167.853939	C8H10NO6P
Methylergometrine	2325.430439	C20H25N3O2
Primidone	1256.205283	C12H14N2O2
Valinomycin	986.4817999	C54H90N6O18
Benserazide	702.8249232	C10H15N3O5
NSC25485	669.392069	C29H44O12
DL-METHIONINE	489.4099827	CH3S(CH2)2CH(NH2)COOH

Abbreviation: DL-METHIONINE, DL-2-amino-4-(methylthio) butyric acid.

Table 3 Binding Energy of Potential Drugs and Key Genes

Drug Name	Gene Name	BE
SCHEMBL14520730	EIF3K	−7.3
Clindamycin	EIF3K	−6.1
NSC25485	EIF3K	−6.9
SCHEMBL14520730	SHMT2	−8.7
Clindamycin	SHMT2	−7.2
Uracil	SHMT2	−5.2
Pyridoxal phosphate	SHMT2	−6.7
Methyler gonovine	SHMT2	−8.5
Primidone	SHMT2	−7.5
Benserazide	SHMT2	−7.8
DL-METHIONINE	SHMT2	−4.9

Abbreviations: EIF3K, Eukaryotic translation initiation factor 3 subunit K; SHMT2, Serine Hydroxymethyltransferase 2; DL-METHIONINE, DL-2-amino-4-(methylthio) butyric acid; BE, Binding Energy.

mitochondrial function. Lee et al[38] established osteoporosis models in wild-type C57BL/6 mice and Pink-/mice by ovariectomy and analyzed their bone parameters 4 weeks after surgery. Bone parameter analysis suggested that compared with other groups, the volume fraction, number and thickness of bone trabecular of Pink1-/- mice in OVX group decreased, while the bone trabecular space increased significantly. siRNA silencing of Pink1 in MC3T3-E1 progenitor cells revealed that mitochondrial homeostasis in MC3T-E1 cells was impaired and a large amount of ROS was produced, which severely inhibited its osteogenic differentiation ability. The miR-l8la is highly expressed in osteoporotic mice, and the level of osteoprotegerin (OPG) can be regulated target-oriented to affect osteoclast activity. In conclusion, *SHMT2* may be associated with osteoporosis.[39] The above studies suggest that *SHMT2* may affect OP through mitochondria. This suggests that *SHMT2* may be a potential therapeutic target for OP.

EIF3K is a subunit of the eukaryotic translation initiation factor 3 and may be involved in oxidative stress, which is associated with osteoporosis.[40] EIF3K gene was enriched into chemokine and TGF-β signaling pathways. The SHMT2 gene is enriched into pathways such as cell response to stimuli and metabolism of amino acids and their derivatives. Study found that disc displacement resulted in a significant increase in articular surface pressure and subchondral bone loss through activation of the C-C chemokine ligand 5 (CCL5) chemokine receptor-AKT2 (CCL5-CCRS-AKT2) axis.[41] Inhibition of CCL5 or AKT2 can reduce subchondral bone loss and improve subchondral bone microstructure. Cytological studies have confirmed that CCL5 regulates osteoclast formation by binding to its receptor Catalytic Core Regulators (CCRS) and activating the

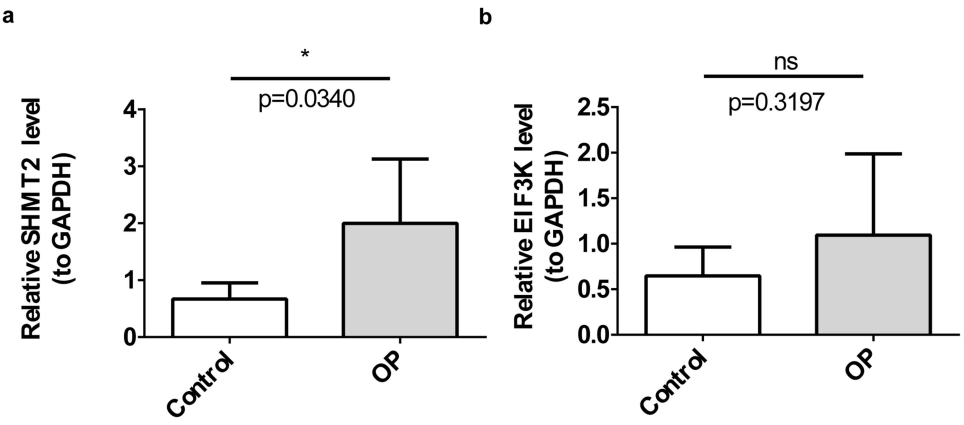

Figure 9 Expression validation of key genes. **(a)** *SHMT2*. **(b)** *EIF3K*. ns, not significant; *, p < 0.05.

https://doi.org/10.2147/ORR.S518036

AKT2 pathway. Interleukin-15 was involved in mediating inflammatory bone loss and bone metabolism by stimulating osteoclast differentiation.[42] Studies have shown that TGF-β/Smad signal transduction is inhibited in the pathological process of osteoporosis, and the decoction of Herba eumedium and Ligustrum can up-regulate the expression of TGF-β1, enhance the phosphorylation of Smad3, inhibit bone resorption, promote bone formation, and alleviate the damage of bone biomechanical properties and trabecular structure in rats with glucocorticoid-induced osteoporosis.[43] In addition, cysteine, as a receptor for the Wnt signaling pathway, plays an important role in the accumulation of bone mass in bone tissue in the body.[44] Various studies have shown that the key genes related to lipophagy, *EIF3K*, and *SHMT2*, may affect the occurrence and development of osteoporosis in patients by affecting chemokine signaling pathway, TGF-β signaling pathway metabolism of amino acids and their derivatives and other pathways.

Activated dendritic cell and mast cell, two types of immune infiltrating cells, showed significant differences between disease and control. Dendritic cell-specific transmembrane protein (DC-STAMP), which was discovered for the first time in human dendritic cells.[45,46] At present, it is generally believed that DC-STAMP is the main regulator of osteoclast fusion process.[47,48] Study[49] shows that in the presence of RANKL and M-CSF, DC-STAMP deficient cells could not produce multinucleated osteoclasts, and DC-STAMP gene knockout mice showed osteosclerosis phenotype due to lack of functional multinucleated osteoclasts. However, after overexpression of DC-STAMP gene by retrovirus, OPC fusion increased. In addition, studies have shown that increased osteoclast activity and bone resorption are associated with the proliferation of bone marrow mast cells. Frame was the first to observe and count bone marrow mast cells in senile osteoporosis patients by using histochemical methods, and found that bone marrow mast cell hyperplasia in senile osteoporosis patients.[50] These studies indicate that activated dendritic cells and mast cells play an important role in OP, which may be an indication of the onset and development of OP.

Autophagy, as an important intracellular degradation and recycling mechanism, degrades damaged organelles, proteins and other cellular components through lysosomes to maintain cell homeostasis and function.[51] In bone cells, this process is equally critical, especially in response to oxidative stress and nutrient deficiencies.[52] For example, studies have shown that chronic hyperglycemia can cause dysfunction in autophagy, resulting in abnormal expression of autophagy-related proteins, and ultimately negatively affect bone health.[53] Recent studies have highlighted that autophagy dysfunction plays a role in these metabolic conditions, and restoration of autophagy function can help restore metabolic homeostasis and rebuild bone fat balance.[54] For example, SP-EVLP promotes osteoblast proliferation through activation of melatonin-induced autophagy.[55] However, most current studies have not focused on the association between lipid autophagy and osteoporosis (OP), and the lack of systematic and in-depth exploration of genes related to lipid autophagy makes it difficult to fully explain the mechanism of lipid autophagy in OP. Unlike this study, few existing studies have constructed complete regulatory networks and predictive drug models by integrating multi-omics analysis, which is lacking in providing comprehensive guidance for clinical diagnosis and treatment. This study focuses on the relationship between lipid autophagy and OP, which has advantages in gene screening and mechanism exploration.

This study identified the key genes EIF3K and SHMT2 involved in lipid autophagy in osteoporosis (OP), which brought important breakthroughs for the clinical diagnosis and treatment of OP. EIF3K and SHMT2 point the way to the development of new therapeutic drugs. For EIF3K, drugs that can accurately regulate its expression can be developed to enhance its effect on antioxidant stress,[56] thus slowing down the OP process. For SHMT2, drugs can be developed to interfere with its metabolic pathways, improve mitochondrial function, and inhibit bone loss.[57] Second, based on the functions and regulatory mechanisms of key genes, personalized treatment programs can be implemented. For patients with abnormal expression of EIF3K and SHMT2, gene therapy, such as RNA interference technology,[58] was used to accurately regulate gene expression. Or combined with traditional drug therapy to enhance the therapeutic effect by regulating key gene-related pathways.[59] Overall, the discovery of EIF3K and SHMT2 opens up a new way for the clinical diagnosis and treatment of OP, and further research is needed in the future to translate these findings into practical clinical applications and bring better treatment prospects for OP patients.

However, there are some limitations to this study. On the one hand, the clinical sample size was relatively small, which may have an impact on statistical power, for example, the difference in EIF3K expression failed to reach the level of significance in qPCR validation. On the other hand, there is a lack of animal experiments and cell function experiments to directly verify the regulatory mechanisms of EIF3K and SHMT2 in lipid phagocytosis and bone

metabolism. In addition, bioinformatic analyses rely mainly on public databases and require further experiments to validate them. In order to promote the progress of research in this area, future studies may consider expanding the clinical sample cohort and combining multi-center data to better verify the stability of genetic markers. At the same time, gene knockout/overexpression models, such as OP mouse models or osteoblast cell lines, were constructed to further clarify the function of key genes. In addition, in vitro and in vivo intervention experiments based on predictive drugs (such as clindamycin) were conducted to evaluate their regulatory effects on bone mineral density and lipid phagocytosis. At the cellular level, gene intervention can be performed in MC3T3-E1 osteoblasts or bone marrow mesenchymal stem cells, and downstream signaling pathways can be resolved in combination with transcriptome sequencing and metabolomics. Finally, a mouse model of osteoporosis (such as ovariectomy and glucocorticoid induction) was established to detect gene expression changes, and histological and biochemical analyses were carried out to lay a more solid foundation for the use of genes in osteoporosis treatment.

Conclusions

In conclusion, this study obtained the key genes EIF3K and SHMT2 associated with lipid autophagy in osteoporosis through bioinformatics screening and expression verification. It is expected to become a new potential therapeutic target for OP and provide new ideas for the study of the molecular mechanism of OP. Of course, this needs to be confirmed by more independent samples and in vivo experiments. If these research results can be further verified, they will provide important theoretical basis and potential intervention direction for the early diagnosis and prevention of OP, and have great significance for improving the prevention and treatment level of OP.

Abbreviations

Lipophagy, Lipid droplet autophagy; OP, Osteoporosis; LRGs, Lipophagy-related genes; DEGs, Differentially expressed genes; LASSO, Least absolute shrinkage and selection operator; RT-qPCR, Real-time fluorescence quantitative PCR; BMD, bone mineral density; WGCNA, Weighted gene co-expression network analysis; SsGSEA, Single-sample gene set enrichment analysis; SVM-RFE, Support vector machine recursive feature elimination; DCA, Decision curve analysis; ROC, Receiver operating characteristic; GO, Gene ontology; KEGG, Kyoto encyclopedia of genes and genes; CCs, Cellular components; BPs, Biological processes; TFs, Transcription factors; MFs, Molecular functions.

Data Sharing Statement

The datasets analysed during the current study are available in the [GEO] repository, [http://www.ncbi.nlm.nih.gov/geo/], [MSigDB] repository, [https://www.gsea-msigdb.org/gsea/msigdb], [ENCODE] repository, [https://www.networkanalyst.ca/faces/home.xhtml], [TarBase] repository, [http://diana.imis.athena-innovation.gr/DianaTools], and [StarBase] repository, [http://starbase.sysu.edu.cn/].

Ethics Approval and Consent to Participate

The principles of the Declaration of Helsinki have been followed in this study involving human participants and approved by the Ethics Committee of The Second People's Hospital of Guiyang (approval number: JYYY-2024-WZ-15). The patients provided their written informed consent to participate in this study.

Acknowledgments

We would like to express our sincere gratitude to all individuals and organizations who supported and assisted us throughout this research. Special thanks to the following authors: Yu Yang, Xiaobing Shi, Qian Zhang, Ji Wu, Runqi Xie, Yu Bi, Bo Lin. In conclusion, we extend our thanks to everyone who has supported and assisted us along the way. Without your support, this research would not have been possible.

Funding

This research received no specific grant from funding agencies in the public, commercial, or not-for-profit sectors.

Disclosure

The authors declare that they have no competing interests in this work.

References

1. Yalaev BI, Novikov AV, Minniakhmetov IR, Khusainova RI. Development of prognostic clinical and genetic models of the risk of low bone mineral density using neural network training. *Probl Endokrinol*. 2024;70(6):67–82. doi:10.14341/probl13421
2. NIH Consensus Development Panel on Osteoporosis Prevention. Diagnosis, and therapy, March 7-29, 2000: highlights of the conference. *South Med J*. 2001;94:569–573.
3. Wang X, Pei Z, Hao T, et al. Prognostic analysis and validation of diagnostic marker genes in patients with osteoporosis. *Front Immunol*. 2022;13:987937. doi:10.3389/fimmu.2022.987937
4. Zhao Y, Yan J, Zhu Y, Han Z, Li T, Wang L. A novel prognostic 6-gene signature for osteoporosis. *Front Endocrinol*. 2022;13:968397. doi:10.3389/fendo.2022.968397
5. Li Q, Zhao Y, Guo H, et al. Impaired lipophagy induced-microglial lipid droplets accumulation contributes to the buildup of TREM1 in diabetes-associated cognitive impairment. *Autophagy*. 2023;19(10):2639–2656. doi:10.1080/15548627.2023.2213984
6. Zhu M, Hao G, Xing J, et al. Bone marrow adipose amount influences vertebral bone strength. *Exp Ther Med*. 2019;17(1):689–694. doi:10.3892/etm.2018.7003
7. Huang JM, Bao Y, Xiang W, et al. Icariin regulates the bidirectional differentiation of bone marrow mesenchymal stem cells through canonical wnt signaling pathway. *Evid Based Complement Alternat Med*. 2017;2017(1):8085325. doi:10.1155/2017/8085325
8. Nandy A, Richards A, Thapa S, Akhmetshina A, Narayani N, Rendina-Ruedy E. Altered osteoblast metabolism with aging results in lipid accumulation and oxidative stress mediated bone loss. *Aging Dis*. 2024;15(2):767–786. doi:10.14336/AD.2023.0510
9. Fujimaki T, Ando T, Hata T, et al. Exogenous parathyroid hormone attenuates ovariectomy-induced skeletal muscle weakness in vivo. *Bone*. 2021;151:116029. doi:10.1016/j.bone.2021.116029
10. He Y, Liu T, Peng X, et al. Molecular mechanism of mitochondrial autophagy mediating impaired energy metabolism leading to osteoporosis. *Biochim Biophys Acta Mol Basis Dis*. 2025;1871(3):167685. doi:10.1016/j.bbadis.2025.167685
11. He H, Zhang Y, Sun Y, et al. Folic acid attenuates high-fat diet-induced osteoporosis through the AMPK signaling pathway. *Front Cell Dev Biol*. 2022;9:791880. doi:10.3389/fcell.2021.791880
12. Liang X, Hou Z, Xie Y, et al. Icariin promotes osteogenic differentiation of bone marrow stromal cells and prevents bone loss in OVX mice via activating autophagy. *J Cell Biochem*. 2019;120(8):13121–13132. doi:10.1002/jcb.28585
13. Rendina-Ruedy E, Guntur AR, Rosen CJ. Intracellular lipid droplets support osteoblast function. *Adipocyte*. 2017;6(3):250–258. doi:10.1080/21623945.2017.1356505
14. Ji C, Zhang Z, Xu X, Song D, Zhang D. Hyperlipidemia impacts osteogenesis via lipophagy. *Bone*. 2023;167:116643. doi:10.1016/j.bone.2022.116643
15. Jiang B, Mou YJ, Zhang XM, et al. Ziyin bushen fang improves diabetic osteoporosis by inhibiting autophagy and oxidative stress in vitro and in vivo. *Comb Chem High Throughput Screen*. 2024;27(5):786–796. doi:10.2174/0113862073261310231113062630
16. Hänzelmann S, Castelo R, Guinney J. GSVA: gene set variation analysis for microarray and RNA-seq data. *BMC Bioinf*. 2013;14:7. doi:10.1186/1471-2105-14-7
17. Langfelder P, Horvath S. WGCNA: an R package for weighted correlation network analysis. *BMC Bioinf*. 2008;9:559. doi:10.1186/1471-2105-9-559
18. Ritchie ME, Phipson B, Wu D, et al. limma powers differential expression analyses for RNA-sequencing and microarray studies. *Nucleic Acids Res*. 2015; 43:e47.
19. Gustavsson EK, Zhang D, Reynolds RH, Garcia-Ruiz S, Ryten M. ggtranscript: an R package for the visualization and interpretation of transcript isoforms using ggplot2. *Bioinformatics*. 2022;38:3844–3846. doi:10.1093/bioinformatics/btac409
20. Gu Z, Hübschmann D. Make interactive complex heatmaps in R. *Bioinformatics*. 2022;38:1460–1462. doi:10.1093/bioinformatics/btab806
21. Yu G, Wang LG, Han Y, He QY. clusterProfiler: an R package for comparing biological themes among gene clusters. *Omics*. 2012;16:284–287. doi:10.1089/omi.2011.0118
22. Friedman J, Hastie T, Tibshirani R. Regularization paths for generalized linear models via coordinate descent. *J Stat Softw*. 2010;33:1–22. doi:10.18637/jss.v033.i01
23. Wang X, Jiang G, Zong J, et al. Revealing the novel ferroptosis-related therapeutic targets for diabetic foot ulcer based on the machine learning. *Front Genet*. 2022;13:944425. doi:10.3389/fgene.2022.944425
24. Sachs MC. plotROC: a tool for plotting ROC curves. *J Stat Softw*. 2017;79:2. doi:10.18637/jss.v079.c02
25. Zhou G, Soufan O, Ewald J, Hancock REW, Basu N, Xia J. NetworkAnalyst 3.0: a visual analytics platform for comprehensive gene expression profiling and meta-analysis. *Nucleic Acids Res*. 2019;47:W234–W41. doi:10.1093/nar/gkz240
26. Skoufos G, Kakoulidis P, Tastsoglou S, et al. TarBase-v9.0 extends experimentally supported miRNA-gene interactions to cell-types and virally encoded miRNAs. *Nucleic Acids Res*. 2024;52:D304–D10. doi:10.1093/nar/gkad1071
27. Li JH, Liu S, Zhou H, Qu LH, Yang JH. starBase v2.0: decoding miRNA-ceRNA, miRNA-ncRNA and protein-RNA interaction networks from large-scale CLIP-Seq data. *Nucleic Acids Res*. 2014;42:D92–7. doi:10.1093/nar/gkt1248
28. Shannon P, Markiel A, Ozier O, et al. Cytoscape: a software environment for integrated models of biomolecular interaction networks. *Genome Res*. 2003;13:2498–2504. doi:10.1101/gr.1239303
29. Seeliger D, de Groot BL. Ligand docking and binding site analysis with PyMOL and autodock/vina. *J Comput Aided Mol Des*. 2010;24:417–422. doi:10.1007/s10822-010-9352-6
30. Greenhill C. Bone: autophagy regulates bone growth in mice. *Nat Rev Endocrinol*. 2016;12:4.
31. Bo T, Yan F, Guo J, et al. Characterization of a relatively malignant form of osteopetrosis caused by a novel mutation in the PLEKHM1 gene. *J Bone Miner Res*. 2016;31:1979–1987. doi:10.1002/jbmr.2885
32. Shin NY, Choi H, Neff L, et al. Dynamin and endocytosis are required for the fusion of osteoclasts and myoblasts. *J Cell Biol*. 2014;207:73–89. doi:10.1083/jcb.201401137

33. DeSelm CJ, Miller BC, Zou W, et al. Autophagy proteins regulate the secretory component of osteoclastic bone resorption. *Dev Cell*. 2011;21:966–974. doi:10.1016/j.devcel.2011.08.016
34. Lin NY, Chen CW, Kagwiria R, et al. Inactivation of autophagy ameliorates glucocorticoid-induced and ovariectomy-induced bone loss. *Ann Rheum Dis*. 2016;75:1203–1210. doi:10.1136/annrheumdis-2015-207240
35. Salsman J, Pinder J, Tse B, Corkery D, Dellaire G. The translation initiation factor 3 subunit eIF3K interacts with PML and associates with PML nuclear bodies. *Exp Cell Res*. 2013;319(17):2554–2565. doi:10.1016/j.yexcr.2013.09.001
36. Minton DR, Nam M, McLaughlin DJ, et al. Serine catabolism by SHMT2 is required for proper mitochondrial translation initiation and maintenance of formylmethionyl-tRNAs. *Mol Cell*. 2018;69:610–21.e5. doi:10.1016/j.molcel.2018.01.024
37. Morscher RJ, Ducker GS, Li SH, et al. Mitochondrial translation requires folate-dependent tRNA methylation. *Nature*. 2018;554:128–132. doi:10.1038/nature25460
38. Lee SY, An HJ, Kim JM, et al. PINK1 deficiency impairs osteoblast differentiation through aberrant mitochondrial homeostasis. *Stem Cell Res Ther*. 2021;12:589. doi:10.1186/s13287-021-02656-4
39. De Martinis M, Ginaldi L, Allegra A, et al. The osteoporosis/microbiota linkage: the role of miRNA. *Int J Mol Sci*. 2020;21:8887. doi:10.3390/ijms21238887
40. Xu S, Khoo S, Dang A, et al. Differential regulation of mitogen-activated protein/ERK kinase (MEK)1 and MEK2 and activation by a Ras-independent mechanism. *Mol Endocrinol*. 1997;11:1618–1625. doi:10.1210/mend.11.11.0010
41. Feng SY, Lei J, Li YX, et al. Increased joint loading induces subchondral bone loss of the temporomandibular joint via the RANTES-CCRs-Akt2 axis. *JCI Insight*. 2022;7:e158874. doi:10.1172/jci.insight.158874
42. Koh JM, Oh B, Ha MH, et al. Association of IL-15 polymorphisms with bone mineral density in postmenopausal Korean women. *Calcif Tissue Int*. 2009;85:369–378. doi:10.1007/s00223-009-9290-2
43. Yang Y, Nian H, Tang X, Wang X, Liu R. Effects of the combined herba epimedii and fructus ligustri lucidi on bone turnover and TGF-β1/Smads pathway in GIOP rats. *J Ethnopharmacol*. 2017;201:91–99. doi:10.1016/j.jep.2017.02.033
44. Williams BO, Insogna KL. Where Wnts went: the exploding field of Lrp5 and Lrp6 signaling in bone. *J Bone Miner Res*. 2009;24:171–178. doi:10.1359/jbmr.081235
45. Chiu YH, Mensah KA, Schwarz EM, et al. Regulation of human osteoclast development by dendritic cell-specific transmembrane protein (DC-STAMP). *J Bone Miner Res*. 2012;27:79–92. doi:10.1002/jbmr.531
46. Mensah KA, Ritchlin CT, Schwarz EM. RANKL induces heterogeneous DC-STAMP(lo) and DC-STAMP(hi) osteoclast precursors of which the DC-STAMP(lo) precursors are the master fusogens. *J Cell Physiol*. 2010;223:76–83. doi:10.1002/jcp.22012
47. Chiu YH, Ritchlin CT. DC-STAMP: a key regulator in osteoclast differentiation. *J Cell Physiol*. 2016;231:2402–2407. doi:10.1002/jcp.25389
48. Wisitrasameewong W, Kajiya M, Movila A, et al. DC-STAMP is an osteoclast fusogen engaged in periodontal bone resorption. *J Dent Res*. 2017;96(6):685–693. doi:10.1177/0022034517690490
49. Yagi M, Miyamoto T, Sawatani Y, et al. DC-STAMP is essential for cell-cell fusion in osteoclasts and foreign body giant cells. *J Exp Med*. 2005;202(3):345–351. doi:10.1084/jem.20050645
50. Frame B, Nixon RK. Bone-marrow mast cells in osteoporosis of aging. *N Engl J Med*. 1968;279(12):626–630. doi:10.1056/NEJM196809192791203
51. Mizushima N, Komatsu M. Autophagy: renovation of cells and tissues. *Cell*. 2011;147(4):728–741. doi:10.1016/j.cell.2011.10.026
52. Lemasters JJ. Selective mitochondrial autophagy, or mitophagy, as a targeted defense against oxidative stress, mitochondrial dysfunction, and aging. *Rejuvenation Res*. 2005;8(1):3–5. doi:10.1089/rej.2005.8.3.
53. Jiang L, Song X, Yan L, Liu Y, Qiao X, Zhang W. Molecular insights into the interplay between type 2 diabetes mellitus and osteoporosis: implications for endocrine health. *Front Endocrinol*. 2025;15:1483512. doi:10.3389/fendo.2024.1483512
54. Zhang B, Cui J, Zhang X, et al. Autophagy: regulating the seesaw of bone-fat balance. *Front Cell Dev Biol*. 2025;13:1465092. doi:10.3389/fcell.2025.1465092
55. Lu J, Chen J, Jiang Y, et al. Ancient medicinal insect steleophaga plancyi (boleny)-derived extracellular vesicle-like particles enhances autophagic activity to promote osteogenic differentiation via melatonin in osteoporosis. *Int J Nanomed*. 2025;20:2059–2071. doi:10.2147/IJN.S505443
56. Duan H, Zhang S, Zarai Y, et al. eIF3 mRNA selectivity profiling reveals eIF3k as a cancer-relevant regulator of ribosome content. *EMBO J*. 2023;42(12):e112362. doi:10.15252/embj.2022112362.
57. Ron-Harel N, Santos D, Ghergurovich JM, et al. Mitochondrial biogenesis and proteome remodeling promote one-carbon metabolism for T cell activation. *Cell Metab*. 2016;24(1):104–117. doi:10.1016/j.cmet.2016.06.007
58. Lundstrom K. Special issue: gene therapy with emphasis on RNA interference. *Viruses*. 2015;7(8):4482–4487. doi:10.3390/v7082830
59. Salgado R, Moore H, Martens JWM, et al. IBCD-faculty. Societal challenges of precision medicine: bringing order to chaos. *Eur J Cancer*. 2017;84:325–334. doi:10.1016/j.ejca.2017.07.028